JOURNAL OF MATERIALS SCIENCE **38** (2003) 1471 – 1477

CN_x/TiN_y films prepared by ion-beam sputtering

D. L. YU, J. L. HE, S. M. LIU, D. C. LI, Y. J. TIAN*
Key Laboratory of Metastable Materials Science and Technology, Hebei, Yanshan University, Qinhuangdao 066004, People's Republic of China; College of Materials Science and Engineering, Yanshan University, Qinhuangdao 066004, People's Republic of China
E-mail: fhcl@ysu.edu.cn

O. YANAGISAWA
Faculty of Engineering, Hiroshima University, Hiroshima, Japan

CN_x/TiN_y multilayers were prepared by ion-beam sputtering and analyzed by X-ray diffraction (XRD), transmission electron microscopy (TEM), selected area electron diffraction (SAED), energy-dispersive X-ray (EDX). EDX results show that the atom ratios of [N]/([C] + [N] + [Ti]) in the multilayers vary from 20 at.% to 41 at.%. XPS analysis presents that the N content of the CN_x layer in CN_x/TiN_y is about 32.18 at.%. The nature of chemical bonding of the CN_x layer in CN_x/TiN_y was also analyzed. The X-ray and electron diffraction analyses suggest that three kinds of C_3N_4 phases, such as β-C_3N_4, graphite-C_3N_4 and cubic-C_3N_4, are embodied in the multilayers. In CN_x/TiN_y bilayers, a hetero-epitaxial relationships, of (1 1 2) cubic-C_3N_4//(1 1 13) Ti_2N, and [42 $\bar{3}$] cubic-C_3N_4//[1 $\bar{1}$ 0] Ti_2N, was observed between cubic-C_3N_4 and Ti_2N.

1. Introduction

Over the past decade, studies of carbon nitride compounds have been of great interest in the fields of materials science and engineering. Various deposition techniques have been employed as the synthesis method of carbon nitrides, including reactive magnetron sputtering [1], pulsed laser ablation deposition [2], combined radio-frequency (RF) and direct-current (DC) plasma beam deposition [3], ion-beam-assisted deposition [4], hot-filament chemical vapor deposition [5], high-current vacuum arc deposition [6], electron cyclotron resonance assisted chemical vapor deposition [7], and ion-beam sputtering deposition [8]. On the basis of calculated results by Cohen [9] and Teter [10], we know that the carbon nitride crystals with any structure are metastable. In order to obtain metastable carbon nitride crystals in the CN film, many solid materials, such as Si, Ni, KCl, TiN, ZrN, WN, and Si_3N_4, have been applied as templates to investigate the possibility of synthesizing carbon nitride compounds. Some researchers [11–13] claimed that they obtained crystalline C_3N_4 phases in the multilayers of CN/TiN, CN_x/ZrN, CN/Si_3N_4/Si, CN/Si_3N_4/TiN/Si, CN/Si_3N_4/ZrN/Si etc. However, the sizes of these so-called crystalline C_3N_4 are only a scale of nanometers. We also prepared CN_x/TiN_y multilayers using ion-beam sputtering and reported results on the structural characterization of the graphite-C_3N_4 in the CN_x/TiN_y multilayers by selected area electron diffraction and X-ray diffraction [14]. In this study, we present further results on the investigation crystal structures and compositions of CN_x/TiN_y multilayers and an epitaxial relationship between cubic-C_3N_4 and Ti_2N in CN_x/TiN_y bilayer.

2. Experiment

CN_x/TiN_y multilayers were deposited on NaCl slices and Si(111) wafers, respectively, using an ion-beam sputtering system shown in Fig. 1. The system includes three Kaufman ion sources and a rotatable substrate holder. The construction materials of grids in the ion sources are molybdenum. Two targets of graphite and titanium are used in this study. The targets with sizes of $110 \times 100 \times 4$ mm^3 cover entirely the holder to avoid sputtering it. The discharge gas is high-purity nitrogen (99.999%). The total gas pressure in the chamber is maintained at $4–7 \times 10^{-2}$ Pa with a base pressure of 5×10^{-4} Pa. Before introduced into the sputtering system, all substrates were ultrasonically cleaned in acetone, ethanol, and de-ionized water. In fact the substrates were put on a small mesa over 5 mm above sample holder to dodge the recoil particles from the surface of the holder. The titanium and graphite targets are sputtered alternately to form CN_x/TiN_y multilayers. The thicknesses of CN_x and TiN_y layers are about 25–30 nm and 15–20 nm, respectively. The deposition temperature is about 80°. A very thin plane-view sample of $TiN_y/CN_x/TiN_y$ trilayers or CN_x/TiN_y bilayers deposited on NaCl was used for the TEM analysis. The samples were collected onto a microscope grid after cleaned repeatedly in de-ionized water that dissolves the NaCl substrate. TEM and SAED experiments are

*Author to whom all correspondence should be addressed.

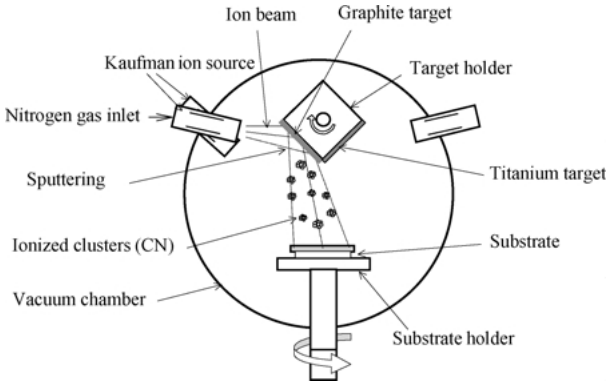

Figure 1 Schematic diagram of ion-beam sputtering system.

performed by H-800 microscope under the condition of accelerating voltage of 150–175 kV. The compositions of the multilayers were studied by EDX (Sigma Kever-Lever 4) attached to the scanning electron microscopy model KYKY2800. The C–N bonding natures and the compositions of CN_x layers were determined in VG ESCALAB 220i-XL photoelectron spectrometer using Mg K_α (1253.6 eV) X-ray source. XPS spectra were collected at pass energy of 40 eV and step of 50 meV.

3. Results and discussion

We firstly investigated the composition of CN_x/TiN_y multilayers by means of EDX and XPS. EDX measurements show that the average N content measured at different regions in the CN_x/TiN_y multilayers varies from 20 at.% to 41 at.%. Besides the three elements of carbon, nitrogen, and titanium, a small amount of oxygen is contained in the multilayers. We consider that the oxygen come from the pollution on surface of CN_x/TiN_y multilayers, which was only lightly cleaned by argon ion beam to mitigate the irradiation damage of the crystals in CN layer. However, the N content obtained from EDX cannot present the real N content of the CN layer because the thickness of the CN layer is only 25–30 nm. Micro-composition analyses show that the some particles of sizes above 200 nm in the CN_x/TiN_y bilayers are mainly made of C, N and Ti. The N contents are about from 34 at.% to 52 at.%. These results indicate that the N content in the CN_x/TiN_y multilayers is uneven. By this token, nitride particles might be randomly distributed in the multilayers.

The chemical bond and the average N content of CN_x layer in the multilayers were analysed by means of XPS. The data of the deconvolution procedure for the spectra (C1s and N1s spectra) shown in Fig. 2 are listed in Table I. Most of our data are similar to that obtained by Bhattacharyya *et al.* [15–20]. N content and N/C of CN_x layer are 32.18 at.% and 0.478 calculated from XPS data, respectively. The XPS results also indicates that main chemical bond in the CN layer are both C–N and C=N bonds. In the predicted α, β and cubic-C_3N_4 crystals, each C atom is sp^3-hybridized and forms C–N single bond (σ-bond) with four N atoms. Each N atom is sp^2-hybridized and σ-bonded with three C atoms. In the graphite C_3N_4 phase, however, each C atom is sp^2-hybridized and σ-bonded with three N atoms. In the

TABLE I Quantification data for C1s and N1s spectra

C1s			N1s		
Binding energy (eV)	[AT]%	Bonding type	Binding energy (eV)	[AT]%	Bonding type
291.36	1.791	π-π* (C)	402.01	3.285	NO
289.17	5.564	CO	400.86	13.947	NO
287.39	21.701	C–N	399.56	52.211	C=N
285.69	48.585	C=N	398.39	30.557	C–N
284.45	15.774	Pure C			
281.99	6.585	Carbides			

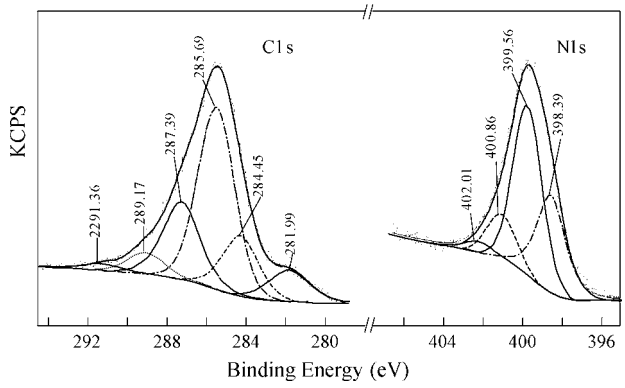

Figure 2 XPS spectra of the CN_x layer in CN_x/TiN_y multilayers.

planar network of hexagonal lattice, each carbon atom forms the π bonding between the interplanar C and N atoms (C=N double bonds). For the arrangement of nitrogen atoms in graphite structure, there are two configurations. First, N atom is σ-bonded with three C atoms, and second, N atom is σ-bonded with two C atoms and π-bonded with one of this two C atoms. According to our XPS data mentioned above, the existence of C–N bond indicates that the α, β or cubic-C_3N_4 phases might form in the CN_x layer, however, C=N bond indicate the formation of graphite C_3N_4 phase. It should be noticed that the C≡N bond was not found in XPS spectra of our sample. The intensity ratios of C–N/C=N in the film reach to 0.447 and 0.585 calculated from the C1s and N1s spectra, respectively.

Basing on the results of EDX and XPS, we speculate that there may be CN crystals in our CN_x/TiN_y multilayers. In order to further make sure this presume, the structure of the multilayers has been characterized by XRD. Fig. 3 shows the XRD spectra obtained from CN_x/TiN_y(18 layers) multilayers deposited on Si(111).

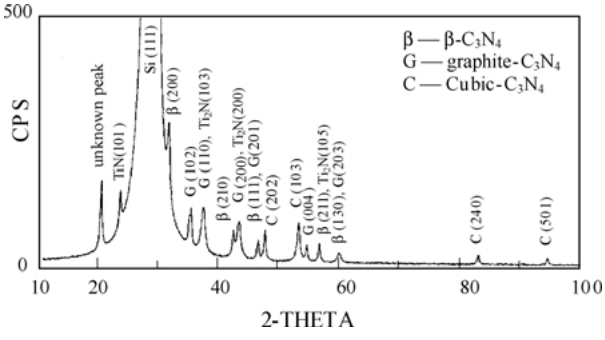

Figure 3 XRD spectrum of CN_x/TiN_y multilayers deposited on Si(111) wafer.

TABLE II Experimental XRD data compared with calculated X-ray diffraction patterns of β-C_3N_4, graphite-C_3N_4, cubic-C_3N_4 and Ti_2N

Experimental	Calculated d (Å)										
	β-C_3N_4			Graphite-C_3N_4			Cubic-C_3N_4			Ti_2N	
d (Å)	hkl	d	I/I_0	hkl	d	I/I_0	hkl	d	I/I_0	hkl	d
3.726										101	3.740
3.378				002	3.36	100					
2.815	200	2.789	100								
2.535				102	2.601	1.1					
2.385				110	2.371	1.2				103	2.396
2.128	210	2.108	33.9								
2.078				200	2.053	3.8				200	2.069
1.944	111	1.958	55.8	201	1.964	19.1					
1.899							202	1.909	56.6		
1.716							103	1.708	1.0		
1.675				004	1.680	7.2					
1.620	211	1.603	14.0							105	1.621
1.539	130	1.547	7.1	203	1.514	6.1					
1.156							240	1.208	6.0		
1.049							501	1.059	12.9		

We calculate the interplanar distances of C_3N_4 phases and the relative intensities ($I/I_0 > 1$) of the powder diffraction based on the latest results of Teter [12]. The results are consistent with the data published in the literature [21]. Table II lists the experimental XRD data and the calculated data. From Table II, we can see that five peaks correspond well with the reflections of (200), (210), (111), (211) and (130) planes of β-C_3N_4 (P3, $a = 6.4017$ Å, $c = 2.4041$ Å), four peaks were matched to the d-spacings of (202), (103), (240) and (501) planes of cubic-C_3N_4 ($I\,\overline{4}\,3d$, $a = 5.3973$ Å), seven peaks correspond with the d-spacings of (002), (102), (110), (200), (201), (004) and (203) planes of graphite-C_3N_4 ($P\,\overline{6}\,m2$, $a = 4.742$ Å, $c = 6.7205$ Å), the four peaks can be fitted to the reflections of (101), (103), (200) and (105) of Ti_2N phase. In addition, one peak with d-spacing of 4.29 Å in the XRD spectrum can be not indexed with the all phases formed by C, N and Ti. Although some diffraction peaks such as peak corresponding to the d-spacing of 4.29 Å can be indexed with α-Si_3N_4, it is difficult for α-Si_3N_4 phase to form under such low temperament. Therefore, we think this is unknown.

In order to speculate the interfacial reaction in the CN_x/TiN_y multilayers, the modulated period (the CN_x/TiN_y bilayer thickness) of the multilayers was calculated by the low angle XRD. We can clearly see five modulation peaks from the low angle XRD pattern of the CN_x/TiN_y multilayers shown in Fig. 4. According to the method introduced in references [22], Bragg equation has following form:

$$\sin^2\theta = (m\lambda)^2/(2L)^2 + 2\delta \quad (1)$$

where m is the serial number of modulation peaks. L is the modulated period (nm). δ is refraction correction. We linearly fit the $\sin^2\theta$ with m^2 shown as Fig. 5 and have got a linear fitting equation:

$$\sin^2\theta = 6.698 \times 10^{-5}\, m^2 + 9.62 \times 10^{-4} \quad (2)$$

Comparing (1) with (2), we can obtain $L = 9.41$ nm. We know the thickness of the CN_x/TiN_y bilayer should be 30–40 nm from deposition rate. This implies that a diffusion of N atoms should happen between CN_x and TiN_y layers. Therefore, we believe that the interfacial diffusion maybe promotes the crystallization of CN_x layer.

There seem a few kinds of C_3N_4 crystals formed in our CN_x/TiN_y multilayers according to the results of XRD analysis. To find these crystals, we finished TEM and SAED experiment of CN_x/TiN_y bilayers. Because the theoretical calculations show that all carbon nitride compounds are amorphous phase and some results also confirmed this viewpoint [23, 24], we avoid using the such fabrication method as ion beam etching for TEM sample, that can cause the phase transition of the carbon nitride crystals exiting in the CN_x/TiN_y multilayers. In this experiment, we use CN_x/TiN_y bilayers deposited on the surface of NaCl as TEM specimen.

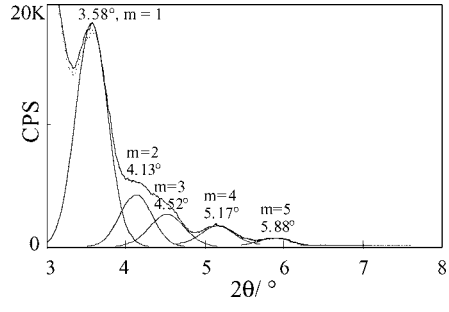

Figure 4 XRD pattern of CN_x/TiN_y multiplayer in low angle range.

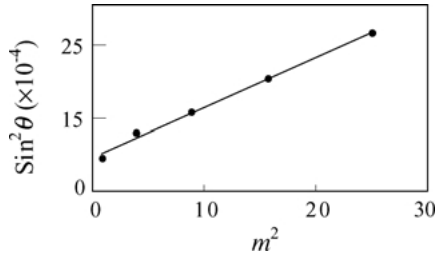

Figure 5 Fitting curve between $\sin^2\theta$ and m^2.

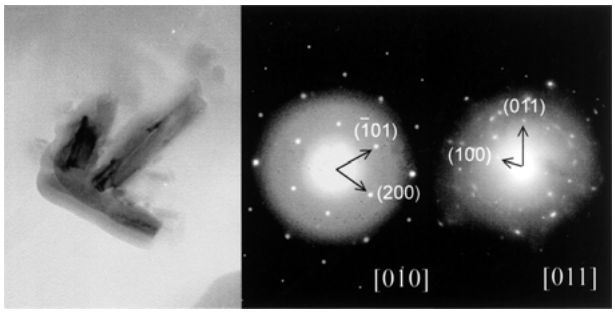

Figure 6 Bright-field image and SAED patterns of strip β-C_3N_4 crystal in the CN_x/TiN_y trilayer.

TABLE III Comparison of the diffraction rings data with the interplanar spacings of (*hkl*) phanes calculated from β-C_3N_4 structure

Miller indices (*hkl*)	Calculated *d* (Å)	SAED measured *d* (Å)
110	3.22	3.10
101	2.26	2.28
111	1.96	1.97
220	1.61	1.67
310	1.55	1.55
221	1.35	1.36
320	1.28	1.28
410	1.22	1.20
420	1.05	1.01

The TEM images and SAED analyses show that the CN_x/TiN_y bilayers are composed of an amorphous matrix and some crystals. These crystal sizes range from a few nanometers to 5.0 μm in diameter. Some larger irregular crystals were identified as graphite-C_3N_4 phase. More details about graphite-C_3N_4 phase formed in CN_x/TiN_y multilayers were published in the references [14]. Fig. 6 presents the TEM micrographs of the strip crystals and their two SAED patterns obtained by tilting this sample. They matched well to [010] and [011] crystal axes of the β-C_3N_4 phases, respectively. Besides, we also found some small β-C_3N_4 crystals with the shape of ball shown in Fig. 7. From the SAED pattern, we can see that 9 electron diffraction rings correspond to interplanar distances of (110), (101), (111), (220), (310), (221), (320), (410) and (420) planes of β-C_3N_4 crystal. The electron diffraction data and calculated interplanar distances of β-C_3N_4 were listed in Table III.

Fig. 8 shows the bright field image of some small crystals in another area of the CN_x/TiN_y trilayer and their electron diffraction rings. The ring data listed in the Table IV indicate that these small crystals are composed of cubic-C_3N_4 and Ti_2N phases. In addition, as shown in Fig. 9, we also found some crystals with the shapes corresponding to the equal axis crystal system (fcc). From TEM observation, we can see some detailed structures such as the core and edges (as Fig. 9b and c), which show that the crystals may be three-dimensional.

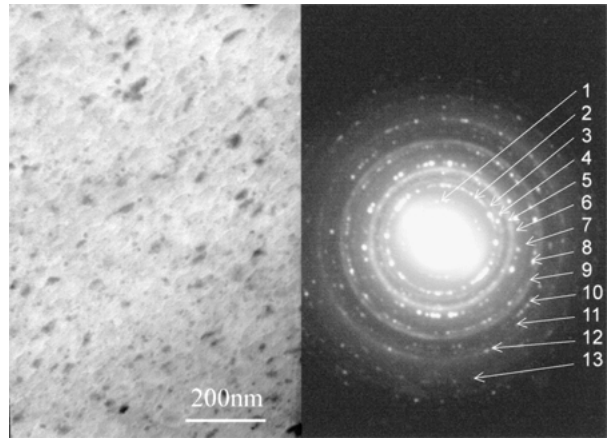

Figure 8 TEM image and diffraction rings of small cubic-C_3N_4 crystal in CN_x/TiN_x trilayer.

They have regular shapes and the size of 200–400 nm. The SAED patterns of these crystals can be indexed with the cubic-C_3N_4 phase.

For the crystals obtaining the core in the CN_x/TiN_y trilayer, we studied its structure in detail by TEM. Fig. 10 presents the TEM image of one of these crystals and its two SAED patterns obtained by rotating this crystal. The two SAED patterns were indexed and correspond to [0$\bar{1}$1] and [112] crystal axes of cubic-C_3N_4, respectively. However, when enlarging Fig. 10c, we can find that it is made

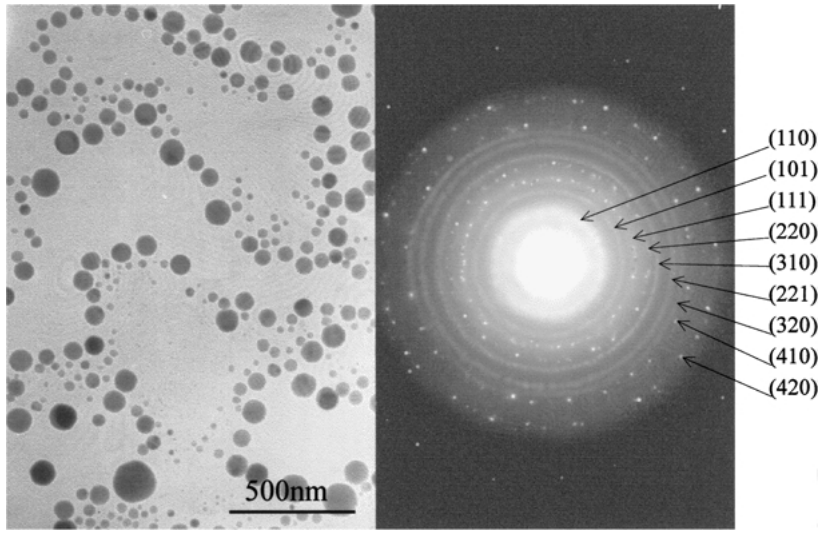

Figure 7 The image and diffraction rings of β-C_3N_4 crystals with the shape of small ball.

TABLE IV Comparison of measured *d*-spacing of the SAED with the calculated values of cubic- C_3N_4 and X-ray powder diffraction data (XRPDD) from the JCPDS of Ti_2N. (No. 23-1455)

	SAED-measured		Calculated for cubic-C_3N_4			XRPDD for Ti_2N		
Number	*D* (nm)	Intensity	*D* (nm)	*hkl*	Intensity	*D* (nm)	*hkl*	Intensity
1	0.377	w				0.3740	101	w
2	0.266	vs						
3	0.237	w				0.2396	103	vw
4	0.218	m	0.2203	221	vs	0.2200	004	m
5	0.207	s				0.2069	200	s
6	0.188	s	0.1908	220	s			
7	0.165	vw	0.1707	310	w			
8	0.153	m				0.1508	204	m
9	0.145	m	0.1443	321	m	0.1464	220	m
10	0.134	m	0.1349	400	m			
11	0.127	vw				0.1277	215	vw
12	0.119	w	0.1207	420	w	0.1204	107	vw
13	0.107	w	0.1102	422	m			

Vs, s, m, w, vw represent very strong, strong, mediumweak and very weak diffraction.

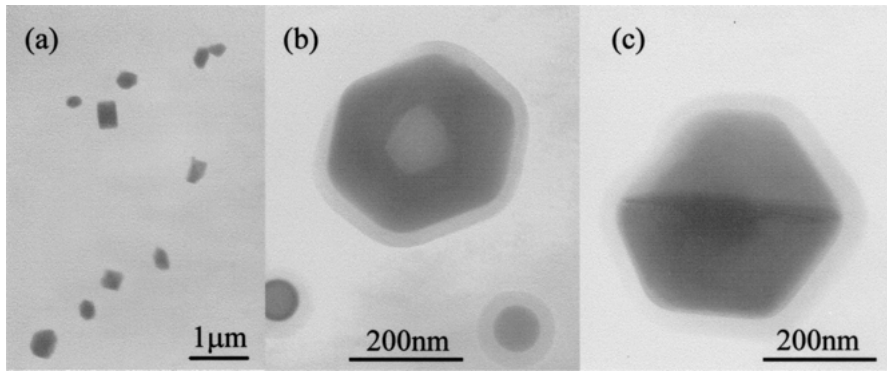

Figure 9 TEM images of some CN crystals in CN_x/TiN_y bilayer. (a) Images of the crystal with several shapes. (b) and (c) Enlarged images show the micrographs of the single crystals.

of two SAED patterns overlapping each other shown as Fig. 11. The identification results show that one fits well to the [112] crystal axis of cubic-C_3N_4, and the other fits well to the [113] crystal axis of Ti_2N. The structural parameter of cubic-C_3N_4 with the space group $I\ \bar{4}\ 3d$ (no. 220) is $a = 5.3973$ Å and its unit cell is shown in Fig. 12a. The structural parameters of Ti_2N with the space group *I41/amd* (no. 141) are $a = 4.140$ Å and $c = 8.805$ Å and its unit cell is shown in Fig. 13a. On the basis of crystal structure analysis, we know that the (1 1 2) plane is normal to the [112] direction in the cubic-C_3N_4 crystal and that the (1 1 13) plane is normal to the [113] direction in Ti_2N crystal.

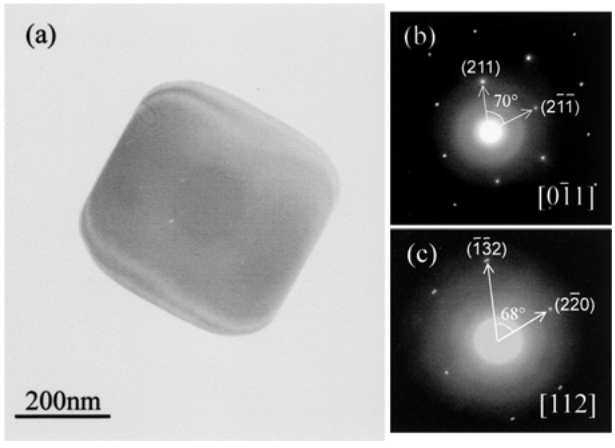

Figure 10 TEM bright-field image and SAED patterns of the cubic-C_3N_4 crystal in the CN_x/TiN_y bilayers deposited on the NaCl substrate. (a) Image shows a crystal containing a nucleus. (b) SAED patterns correspond with [0$\bar{1}$1] axis of cubic-C_3N_4. (c) SAED patterns correspond with [112] axis of cubic-C_3N_4.

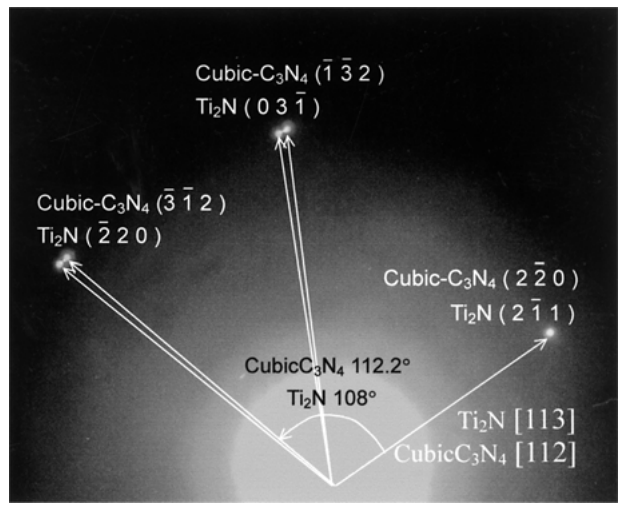

Figure 11 Fig. 10(c) enlarged show that the SAED pattern of [112] axis of cubic-C_3N_4 laps over the SAED pattern of [113] axis of Ti_2N.

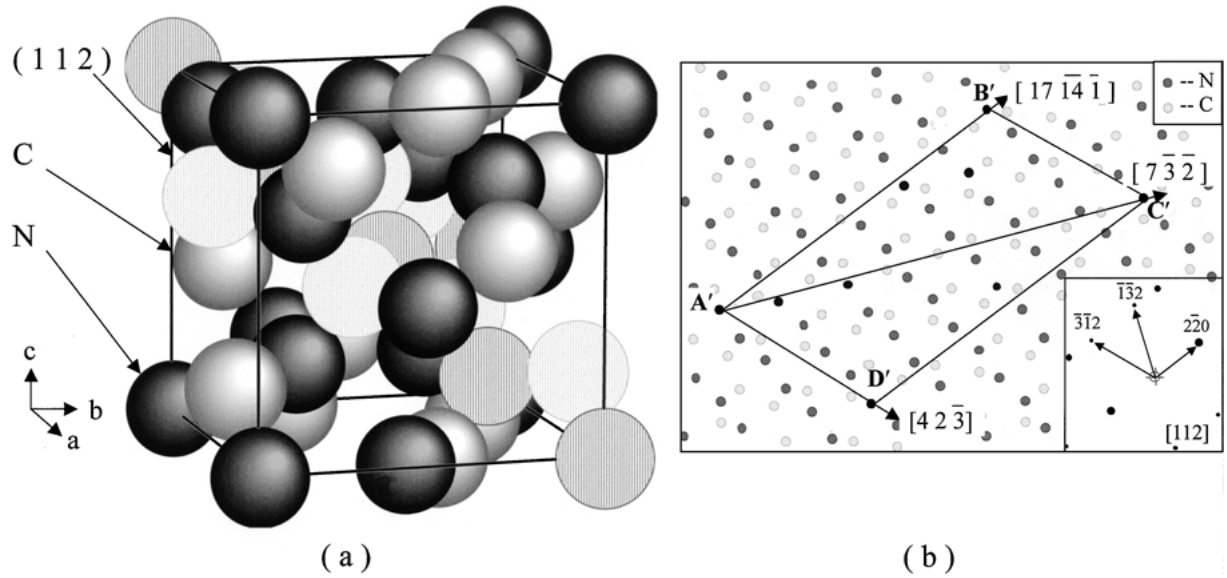

Figure 12 The crystal structures of cubic-C_3N_4 ($I\ \bar{4}\ 3d$). (a) The unit cell of cubic-C_3N_4. (b) Atomic positions and the nets on (112) plane of cubic-C_3N_4.

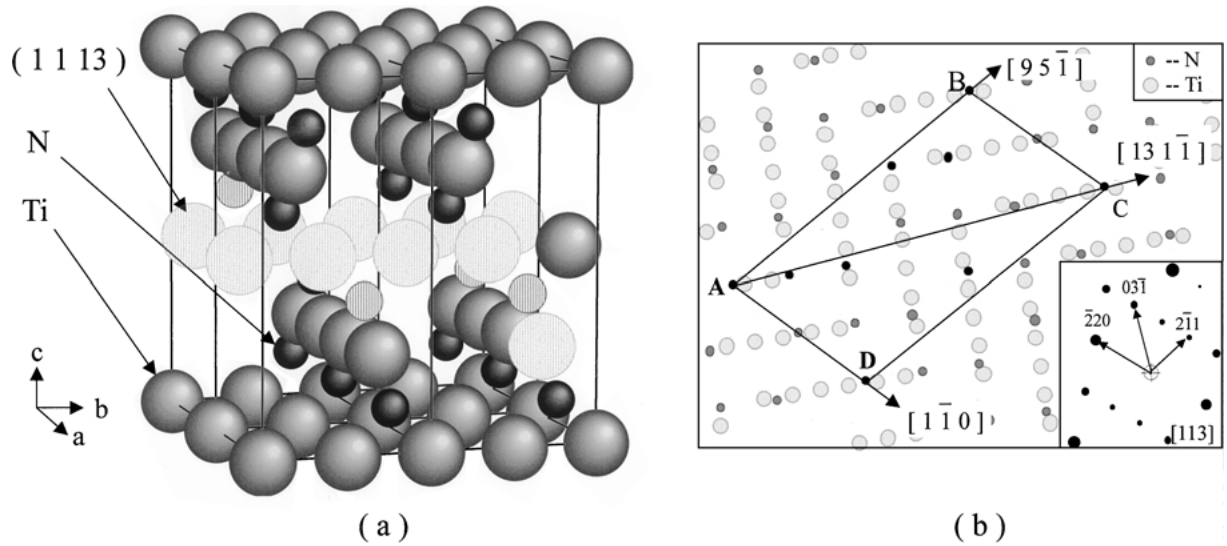

Figure 13 The crystal structures of Ti_2N (*I41/amd*). (a) The unit cells of Ti_2N. (b) Atomic positions and the nets on (1 1 13) plane of Ti_2N.

Using the simulation software of CaRIne Crystallography 3-1, we obtain the atomic arrangements on the cubic-C_3N_4 (1 1 2) plane and the Ti_2N (1 1 13) plane as shown in Figs 12b and 13b. The calculated electron diffraction patterns corresponding to the special axes of two crystals are agreement to the experiment data. Simulation results show that the epitaxy phenomenon between the two planes mentioned above appears at corresponding N atomic positions. Comparing the atomic arrangements on the cubic-C_3N_4 (1 1 2) and the Ti_2N (1 1 13) planes, we can find that A′B′C′D′ net in the cubic-C_3N_4 (112) plane corresponds to the ABCD net in (1 1 13) plane of Ti_2N. It can be seen that 8 atomic positions are well matched between the two lattices. Hence, we think that a hetero-epitaxial relationship may exist between cubic-C_3N_4 and Ti_2N as (1 1 2) cubic-C_3N_4//(1 1 13) Ti_2N and $[42\bar{3}]$ cubic-C_3N_4//$[1\bar{1}0]$ Ti_2N.

In order to confirm the existence of this epitaxial relationship, the lattice misfit was calculated using Bramfitt′s lattice misfit method [25]. Bramfitt′s two-dimensional lattice misfit δ is defined as

$$\delta_{(hkl)_n}^{(hkl)_s} = \sum_{i=1}^{3} \left[\left(|d_{[\mathrm{UVW}]_s^i} \cos\theta - d_{[\mathrm{UVW}]_n^i}| / d_{[\mathrm{UVW}]_n^i} \right) / 3 \right] \times 100\% \quad (3)$$

where n and s refer to the overgrowth plane of film and the parallel substrate plane, respectively; d is the distance between atoms in the [UVW] direction; and θ is an angle from $[\mathrm{UVW}]_n$ to $[\mathrm{UVW}]_s$. Bramfitt gave some results showing that the best hetero-epitaxy can be obtained when $\delta < 6\%$, and that the phenomenon of epitaxy can not be yielded when $\delta > 12\%$. Our calculated lattice misfit, δ, and correlative parameters of cubic-C_3N_4 and Ti_2N are list in Table V. The calculated $\delta_{(112)_{\text{cubic-}C_3N_4}}^{(1113)_{Ti_2N}}$ is equal to 5.7791%, which indicates

TABLE V Calculated lattice misfit, δ, and the matching relationship between cubic-C_3N_4 and Ti_2N

Matching plane	(1 1 2) cubic-C_3N_4//(1 1 13) Ti_2N		
Matching direction	[42$\bar{3}$] cubic-C_3N_4//[1$\bar{1}$0] Ti_2N	[7 $\bar{3}$ $\bar{2}$] cubic-C_3N_4//[13 1 $\bar{1}$] Ti_2N	[17 $\overline{14}$ $\bar{1}$] cubic-C_3N_4//[95$\bar{1}$] Ti_2N
$d_{[UVW]\text{cubic-}C_3N_4}$ (Å)	12.16	29.98	22.80
$d_{[UVW]Ti_2N}$ (Å)	11.71	27.35	21.76
θ°	3.9	0	2.34
$\delta^{(1113)_{Ti_2N}}_{(112)_{\text{cubic-}C_3N_4}}$		5.7791	

that hetero-epitaxial growth of cubic-C_3N_4 on Ti_2N is possible.

4. Conclusions

We have prepared CN_x/TiN_y multilayers by use of nitrogen-ion-beam sputtering graphite and titanium targets. The structure and composition of multilayers have been characterized by XRD, TEM, SAED, EDX, and XPS. The results show that the multilayers are composed of an amorphous matrix, and that some crystals possibly possess the structures of β-C_3N_4, cubic-C_3N_4, graphite-C_3N_4 and Ti_2N. The sizes of crystals range from several nanometers to 5 μm in diameter. The [N]/([C]+[N]+[Ti]) ratios in the CN_x/TiN_y multilayers vary from 20 at.% to 41 at.%. The N content of the CN_x layer in CN_x/TiN_y is about 32.18 at.%. A possible expitaxial relationship between cubic-C_3N_4 and Ti_2N is observed, it is (1 1 2) cubic-C_3N_4//(1 1 13) Ti_2N and [42$\bar{3}$] cubic-C_3N_4//[1$\bar{1}$0] Ti_2N.

Acknowledgements

We acknowledge financial support from Natural Science Foundation of Hebei Province, P.R.China.

References

1. E. BROITMAN, W. T. ZHENG, H. SJOSTROM, I. IVANOV, J.E. GREENE and J. E. SUNDGREN, *Appl. Phys. Lett.* **72** (1998) 2532.
2. I. N. MIHAILESCU, E. GYORGY, R. ALEXANDRESCU, A. LUCHES, A. PERRONE, C. GHICA, J. WERCKMANN, I. COJOCARU and V. CHUMASH, *Thin Solid Films* **323** (1998) 72.
3. G. DINESCU, E. ALDEA, G. MUSA, M. C. M. VAN DE SANDEN, A. DE GRAAF, C. GHICA, M. GARTNER and A. ANDREI, *ibid.* **325** (1998) 123.
4. F. ROSSI, B. ANDRE, A. VAN VEEN, P. E. MIJNARENDS, H. SCHUT, F. LABOHM, M. P. DELPLANCKE, H. DUNLOP and E. ANGER, *ibid.* **253** (1994) 85.
5. YAN CHEN, LIPING GUO and E. G. WANG, *J. Mater. Sci. Lett.* **16** (1997) 594.
6. J. HARTMANN, P. SIEMROTH, B. SCHULTRICH and B. RAUSCHENBACH, *J. Vac. Sci. Technol.* A **15** (1997) 2983.
7. E. G. WANG, *Progress in Materials Science* **41** (1997) 241.
8. TIAN YONGJUN, REN XUEJUN, YU DONGLI, HE JULONG, ZENG HUARONG, CHEN SHIZHEN and LI DONGCHUN, *Chinese Science Bulletin* **41** (1996) 1038.
9. AMY Y. LIU and MARVIN L. COHEN, *Science* **245** (1989) 841.
10. D. M. TETER and R. J. HEMLEY, *ibid.* **271** (1996) 53.
11. K. M. YU, M. L. COHEN and E. E. HALLER, *Phys. Rev.* B **49** (1994) 5034.
12. YAFEI ZHANG, ZHONGHUA ZHOU and HULIN LI, *Appl. Phys. Lett.* **68** (1996) 634.
13. WU DAWEI, FU DEJUN, *et al.*, *Acta Physical Sinica* **48** (1999) 4904.
14. D. L. YU, R. R. XIAO, Y. J. TIAN, *et al.*, *J. Mater. Sci. Lett.* **19** (2000) 553.
15. S. BHATTACHARYYA, C. CARDINAUD, *J. Appl. Phus.* **83** (1998) 4 491.
16. A. P. DEMENTJEV, A. DE GRAAF, D. I. DOLGIY, *et al.*, *Diamond and Related Materials* **8** (1999) 601.
17. JIN-JEN WU, KUEI-HSIEN CHEN, CHENG-YEN WEN, LI-CHYONG, *et al.*, *J. Mater. Chem.* **10** (2000) 783.
18. YONGQING FU, JUN WEI, BIBO YAN and NEE LAM LOH, *J. Mater. Sci.* **35** (2000) 2215.
19. A. ZOCCO, A. PERRONE, E. D. ANNA and G. LEGGIERI, *Diamond and Related Materials* **8** (1999) 582.
20. M. TERRONES, P. REDLICH, N. GROBERT and S. TRASOBARES, *Adv. Mater.* **11** (1999) 655.
21. JIANBO WANG, JIANLIN LEI and RENHUI WANG, *Physical Review* B **58** (1998) 11890.
22. T. K. BARBEE, in Proceedings of Low Energy X-ray Diagnosties, 1982 AIP Conf. Proc. No. 75, New York, p. 131.
23. JOHN V. BADDING, *Adv. Mater.* **9** (1997) 877.
24. H. MONTIGAUD, B. ANGUY, G. DEMAZEAU, I. ALVES, *et al.*, *J. Mater. Sci.* **35** (2000) 2547.
25. B. L. BRAMFITT, *Met. Trams.* **1** (1970) 1987.

Received 2 April
and accepted 24 December 2002